Effects of Topography on Baroclinic Instability

CHANGHENG CHEN AND IGOR KAMENKOVICH

Rosenstiel School of Marine and Atmospheric Science, University of Miami, Miami, Florida

(Manuscript received 8 August 2010, in final form 11 December 2011)

ABSTRACT

The importance of bottom topography in the linear baroclinic instability of zonal flows on the β plane is examined by using analytical calculations and a quasigeostrophic eddy-resolving numerical model. The particular focus is on the effects of a zonal topographic slope, compared with the effects of a meridional slope. A zonal slope always destabilizes background zonal flows that are otherwise stable in the absence of topography regardless of the slope magnitude, whereas the meridional slopes stabilize/destabilize zonal flows only through changing the lower-level background potential vorticity gradient beyond a known critical value. Growth rates, phase speeds, and vertical structure of the growing solutions strongly depend on the slope magnitude. In the numerical simulations configured with an isolated meridional ridge, unstable modes develop on both sides of the ridge and propagate eastward of the ridge, in agreement with analytical results.

1. Introduction

Generation of mesoscale motions in the World Ocean is characterized by several stages, each involving interactions and energy transfer between motions on various spatial scales. The initial stage of eddy development in a large-scale background flow is traditionally described through the rapid growth of infinitesimal normal-mode perturbations, which can, due to their spatial structure, efficiently extract energy from the large-scale background state (e.g., Pedlosky 1987). The corresponding linear instability theory can provide important insights into the spatial structure of the most rapidly growing (most unstable) modes. This initial stage is followed by nonlinear development during which interactions between linear modes become important. These interactions and the corresponding energy transfer are in large part determined by properties of dominant linear modes. For this reason, the linear analysis is an important stepping stone for understanding the dynamics of fully nonlinear eddying flows.

The above mechanism of eddy generation relies on the presence of a mean potential vorticity (PV) gradient, which preconditions large-scale currents for instability (e.g., Pedlosky 1987) and controls nonlinear evolution of eddying flow. Bottom topography can modify background PV gradient and thus play an important role in the dynamics of eddy formation, as well as the stability of background flows. Several previous studies recognized the importance of the combined effect of a background flow and topographic slopes for baroclinically unstable flows (Blumsack and Gierasch 1972; Mechoso 1980; Isachsen 2011; Pennel et al. 2012). Hart (1975a,b), in a two-layer quasigeostrophic (QG) model on the f plane, showed that a unidirectional zonal slope has a destabilizing effect on a circular gyre and generates an asymmetric mean current. A meridional slope can produce small-scale fluctuations in vertically sheared zonal flows (Steinsaltz 1987). More complex topographic configurations lead to additional dynamical effects. In particular, Samelson and Pedlosky (1990) demonstrated that a zonal flow can become locally unstable due to the presence of a localized meridional slope. Small-scale topography can also significantly impact stability of zonal currents (Reznik and Tsybaneva 1999; Benilov 2001). In the absence of background flows, Samelson (1992) found that free-wave modes become surface intensified in a two-layer QG model with small-scale topography, whose horizontal scale is similar to that of the waves. Hallberg (1997) demonstrated that strong topography significantly impacts vertical structure of linear waves and effectively eliminates the barotropic component of the flow and that the motions in the two layers are coupled when the

Corresponding author address: Igor Kamenkovich, Division of MPO, Rosenstiel School of Marine and Atmospheric Science, University of Miami, 4600 Rickenbacker Causeway, Miami, FL 33149.
E-mail: ikamenkovich@rsmas.miami.edu

DOI: 10.1175/JPO-D-12-0145.1

topographic and planetary vorticity gradients are parallel or antiparallel.

Nonlinear development of eddying flows can substantially impact large-scale stratification and circulation, often leading to the formation of new circulation patterns. An important example of such eddy-driven patterns is zonally elongated coherent structures observed in stratified, rotating fluids, including planetary atmospheres (e.g., Kondratyev and Hunt 1982) and oceans (Nowlin and Klinck 1986; Orsi et al. 1995; Maximenko et al. 2005; Sokolov and Rintoul 2007; van Sebille et al. 2011), as well as in high-resolution comprehensive (e.g., Nakano and Hasumi 2005; Richards et al. 2006) and idealized (e.g., Rhines 1994) numerical simulations. In uniform currents with a purely meridional PV gradient, these patterns take a form of stationary zonal jets, although in more complex configurations these patterns can become nonzonal and time dependent. The dynamics of these multiple zonal jets strongly rely on the action of mesoscale eddies (e.g., Panetta 1993; Rhines 1994; Berloff et al. 2009b; Kamenkovich et al. 2009; Melnichenko et al. 2010). In particular, Berloff et al. (2009a) demonstrated that jet formation is triggered and controlled by the emergence of linear, meridionally oriented (''noodle'') modes, whose structure determines several important properties of final nonlinear solution.

Jet formation relies on the presence of a background PV gradient (e.g., Vallis and Maltrud 1993) and has been shown to be affected by topography. In particular, Thompson (2010) showed that simple sinusoidal topographic features affect jet spacing, pattern variability, and meridional transport properties. Thompson and Sallée (2012) demonstrated that idealized asymmetric zonally orientated ridges destroy the continuity of zonal jets and enhances baroclinicity of eddies downstream of topography. Boland et al. (2012) found that in both barotropic and baroclinic systems, jets become tilted in the presence of a zonal topographic slope and are nearly perpendicular to the barotropic PV gradient.

Our motivation is the need to understand the role of topography in the dynamics of eddies and eddy-driven flow patterns (e.g., zonal jets) in the oceans. In this study, we examine the influence of topographic variations on the linear baroclinic instability of a uniform zonal flow. Our particular focus here is on the effects of zonal topographic slopes; an analysis of meridional slopes is carried out for comparison. This initial linear stage is an essential element in the process of eddy and jet formation, and linearized models have been proven to be useful in describing complex nonlinear interactions (Berloff et al. 2009a). This paper is organized as follows: the model is described in section 2; a necessary instability condition and the dispersion relation for unstable modes in the presence of constant topographic slopes (zonal and meridional) are derived in section 3, where we also discuss the dependence of the most unstable mode on the direction of the mean PV gradient; in section 4, we use a numerical version of the linear model to study the relevance of the constant-slope results of section 3 to more realistic configurations with a meridional topographic ridge; and conclusions are drawn in section 5.

2. The model

We consider a two-layer QG model with bottom topography on the β plane. Potential vorticity q_n in each of the two dynamically active isopycnal layers is governed by

$$\frac{\partial q_n}{\partial t} + J(\psi_n, q_n) = 0 \quad (n = 1, 2), \tag{1}$$

where the layer index starts from the top and ψ_n is the streamfunction in the nth layer. $J(\cdot,\cdot)$ is the Jacobian operator.

We are interested in the baroclinic instability of large-scale zonal ocean currents with a vertical shear and consider a horizontally uniform flow U in the upper layer and a motionless lower layer:

$$\psi_1 = \varphi_1 - Uy, \quad \psi_2 = \varphi_2, \tag{2}$$

where φ_1, φ_2 describe disturbances.

The isopycnal potential vorticities consist of several components: relative vorticity of disturbances, β term, and the stretching terms due to the mean flow, disturbances, and topography. They are presented in sequence in the following equation:

$$q_n = \nabla^2\varphi_n + [\beta_0 - (-1)^n F_n U]y + (-1)^n F_n(\varphi_1 - \varphi_2) + \delta_{n2} f_0 \frac{\eta_b(x,y)}{H_2}, \tag{3}$$

where β_0 is the planetary vorticity gradient, H_n are the depths of the upper and lower layers, $\eta_b(x, y)$ is the spatially varying elevation of bottom topography, $F_n = f_0^2/(g'H_n)$, f_0 is the Coriolis parameter, g' is a reduced-gravity coefficient associated with the density jump between the isopycnal layers, and δ_{n2} is the Kronecker delta. It needs to be pointed out that Eq. (3) is simplified by applying the rigid-lid approximation. For convenience, we also define F as the inverse of the square of the internal Rossby deformation radius: $F = f_0^2(H_1 + H_2)/(g'H_1H_2)$;

and introduce two coefficients: $\alpha_1 = H_2/(H_1 + H_2)$ and $\alpha_2 = H_1/(H_1 + H_2)$. It follows that

$$F_1 = \alpha_1 F, \quad F_2 = \alpha_2 F. \tag{4}$$

3. Linear stability analysis: Analytical study

a. Necessary instability condition

For tractability of the analytical analysis, we consider an inviscid flow over a constant slope. First, by linearizing the PV equations we obtain

$$\left(\frac{\partial}{\partial t} + U\frac{\partial}{\partial x}\right)[\nabla^2\varphi_1 - \alpha_1 F(\varphi_1 - \varphi_2)] + \frac{\partial \varphi_1}{\partial x}(\beta_0 + \alpha_1 FU) = 0, \tag{5}$$

$$\frac{\partial}{\partial t}[\nabla^2\varphi_2 + \alpha_2 F(\varphi_1 - \varphi_2)] + \frac{\partial \varphi_2}{\partial x}(\beta_0 - \alpha_2 FU + S_y) - \frac{\partial \varphi_2}{\partial y}S_x = 0, \tag{6}$$

where $S_x \equiv s_x f_0/H_2 = \partial\eta_b/\partial x f_0/H_2$, $S_y \equiv s_y f_0/H_2 = \partial\eta_b/\partial y f_0/H_2$, s_x and s_y are zonal and meridional topographic slopes, respectively. The normal-mode solutions can be sought in the form $\varphi_n = A_n e^{i(kx+ly-\omega t)}$, which upon substitution yields two coupled algebraic equations for A_1 and A_2:

$$[(\omega - Uk)(k^2 + l^2 + \alpha_1 F) + k(\beta_0 + \alpha_1 FU)]A_1 + \alpha_1 F(Uk - \omega)A_2 = 0, \tag{7}$$

$$\omega\alpha_2 FA_1 + [-\omega(k^2 + l^2 + \alpha_2 F) - k(\beta_0 - \alpha_2 FU) - \kappa]A_2 = 0, \tag{8}$$

where $\kappa = f_0/H_2(\mathbf{K} \times \nabla\eta_b)$, which is proportional to the cross product of wavevector $\mathbf{K} = (k, l)$ and topographic slope $\nabla\eta_b$. The corresponding terms in the PV equation represent vortex tube stretching in the lower layer due to the motion over topography.

In the following section, we derive a necessary instability condition. Multiplying Eqs. (7) and (8) by $\alpha_2 FA_1^*/(U - c)$ and $\alpha_1 FA_2^*/(-c)$, respectively, we get

$$\alpha_2 FK^2|A_1^2| + \alpha_1 F\alpha_2 F(|A_1|^2 - A_1^*A_2) - \frac{\alpha_2 F|A_1|^2(\beta_0 + \alpha_1 FU)}{U - c} = 0, \tag{9}$$

$$\alpha_1 FK^2|A_2^2| + \alpha_1 F\alpha_2 F(|A_2|^2 - A_1A_2^*) - \frac{\alpha_1 F|A_2|^2(\beta_0 - \alpha_2 FU + \kappa/k)}{-c} = 0, \tag{10}$$

where $K^2 = k^2 + l^2$, $c = \omega/k$ and A_n^* are the complex conjugates of A_n. Summing up Eqs. (9) and (10), we have

$$K^2F(\alpha_2|A_1|^2 + \alpha_1|A_2|^2) + \alpha_1\alpha_2F^2[|A_1|^2 + |A_2|^2 - (A_1^*A_2 + A_1A_2^*)] - \frac{\alpha_2 F|A_1|^2(\beta_0 + \alpha_1 FU)}{U - c} - \frac{\alpha_1 F|A_2|^2(\beta_0 - \alpha_2 FU + \kappa/k)}{-c} = 0. \tag{11}$$

Taking the imaginary part of Eq. (11) leads to

$$\left[\frac{\alpha_2 F|A_1|^2(\beta_0 + \alpha_1 FU)}{|U - c|^2} + \frac{\alpha_1 F|A_2|^2(\beta_0 - \alpha_2 FU + \kappa/k)}{|-c|^2}\right]\omega_i = 0, \tag{12}$$

where ω_i is the imaginary part of ω. Growing solutions for $k \neq 0$ can exist only if

$$\left(U + \frac{\beta_0}{\alpha_1 F}\right)\left(U - \frac{\beta_0 + \kappa/k}{\alpha_2 F}\right) > 0. \tag{13}$$

Perturbations with an infinitely long zonal scale, namely $k = 0$, are always stable. It is obvious that such perturbations propagate perpendicular to the mean interface slope between the upper and lower layers and cannot feed on the available potential energy stored in the background stratification.

In the absence of topography, whether or not baroclinic instability can develop is determined by such background parameters as the velocity shear (U), stratification ($\alpha_1 F$ and $\alpha_2 F$), and planetary vorticity gradient (β_0) (Pedlosky 1987). In the presence of topography, the stability properties also strongly depend on the magnitudes of the topographic slope ($\nabla\eta_b$) and the wavevector (k, l), as well as on the relative orientation of these two vectors.

When the topographic slope is purely meridional, κ/k reduces to S_y and is independent of the wavevector magnitude and orientation. The slope exerts a stabilizing/destabilizing effect on zonal background flow through changing the background PV gradient in the lower layer. As in the classical Phillips model with a flat bottom, the flow remains stable for all perturbations as long as U does not exceed critical values:

$$\min\left(-\frac{\beta_0}{\alpha_1 F}, \frac{\beta_0 + S_y}{\alpha_2 F}\right) < U < \max\left(-\frac{\beta_0}{\alpha_1 F}, \frac{\beta_0 + S_y}{\alpha_2 F}\right). \tag{14}$$

Note that the above condition implies that the background PV gradient does not change sign in the vertical.

In the presence of a zonal slope, the stability properties are fundamentally different and become strongly dependent on the wavevector of the perturbation itself. Most importantly, for any combination of background parameters, one can always find a perturbation that satisfies (13) and can, therefore, grow. In particular, even a small zonal slope can destabilize an otherwise stable zonal background flow; a similar situation exists for the background currents that are slightly nonzonal (Kamenkovich and Pedlosky 1996). On the other hand, the stability properties of the perturbations, whose wavevectors are parallel to the direction of the topographic slope, are not affected by topography. In other words, if the flow is stable over a flat bottom, the introduction of topography can destabilize only those modes whose wavevectors have across-slope components; for a purely zonal slope, that means $l \neq 0$. In the study of the effects of short-scale sinusoidal topography on baroclinic instability, Benilov (2001) demonstrated similar results: the perturbations are affected the most if their wavevectors are parallel to the isobaths, while those whose wavevectors are perpendicular to the isobaths are not affected by the topography.

In summary, a topographic slope changes the necessary instability condition through modifying the mean PV gradient in the lower layer. A meridional slope can stabilize a zonal background flow by preventing the meridional PV gradient from changing sign between the layers. A zonal slope generates a zonal component of the background PV gradient, which makes the concept of critical shear largely irrelevant since any zonal background flow over a zonal slope can potentially become unstable.

b. The dispersion relation

The necessary condition for instability (13) can only indicate when a zonal background flow can be potentially unstable: an actual solution is needed for determining if growing solutions indeed exist. Nontrivial solutions for A_1 and A_2 of Eqs. (7) and (8) exist only if the determinant of the coefficients is zero. This condition leads to the dispersion relation:

$$[(k^2 + l^2 + \alpha_1 F)(k^2 + l^2 + \alpha_2 F) - \alpha_1\alpha_2 F^2]\omega^2 - [Uk(k^2 + l^2)^2 - 2k(\beta_0 - \alpha_2 FU)(k^2 + l^2) - \kappa(k^2 + l^2 + \alpha_1 F) - k\beta_0 F(\alpha_1 + \alpha_2)]\omega - k[U(k^2 + l^2) - \beta_0][k(\beta_0 - \alpha_2 FU) + \kappa] = 0. \quad (15)$$

To obtain a quantitative perspective on the effects of topography in the rest of this paper, we set the Coriolis parameter $f_0 = 0.83 \times 10^{-4}\ \mathrm{s}^{-1}$, the background planetary vorticity gradient $\beta_0 = 2 \times 10^{-11}\ \mathrm{m}^{-1}\ \mathrm{s}^{-1}$ and internal Rossby deformation radius equal to 25 km. The isopycnal layers thicknesses are set to $H_1 = 1$ km and $H_2 = 3$ km, unless stated otherwise. In the following we examine the effects of meridional and zonal slopes first on the f plane, which allows us to focus on the effects of topography, and then on the β plane, where we investigate an interplay between the effects of the planetary vorticity gradient and topography.

1) THE f PLANE

Topographic effects are most pronounced in the absence of the planetary vorticity gradient β. We, therefore, analyze these effects on the f plane first. By setting $\beta = 0$ and solving the dispersion relation, we can get the growth rate of unstable waves on the f plane as

$$\omega_i = |k| \frac{\sqrt{-\Delta}}{2K^2(K^2 + F)}, \quad (16)$$

where $\Delta = (K^2 + \alpha_1 F)^2 S^2 + 2UK^2(K^4 + \alpha_1 FK^2 - 2\alpha_1\alpha_2 F^2)S + U^2K^4(K^4 - 4\alpha_1\alpha_2 F^2) < 0$, $S = \kappa/k$. In the flat-bottom case, the background zonal flow is always unstable for sufficiently long wavelengths. The corresponding phase speed, the real part of c, is

$$c_r = \frac{K^2 + 2\alpha_2 F}{2(K^2 + F)} U - \frac{S(K^2 + \alpha_1 F)}{2K^2(K^2 + F)}. \quad (17)$$

The equations reveal at least two interesting properties. First, the waves over a flat bottom propagate in the same direction as the mean current but with $c_r < U$; Eq. (17) suggests that the presence of bottom topography can potentially change both the direction and magnitude of the phase speed. However, as we will see in the following analysis, the most unstable mode always has a phase speed that is slower than the mean current in the top layer. Second, two pairs of oppositely signed U and S result in the same ω_i. In other words, the parameter of importance is the relative orientation of the mean isopycnal slope (which determines the sign of U) with respect to the topographic slope. In the analysis of this section, therefore, it is sufficient to consider an eastward background (EB) flow only.

(i) Meridional slope: $\beta_0 = 0$, $s_x = 0$, and $s_y \neq 0$

When the slope is purely meridional, S reduces to S_y. Figure 1a shows the growth rate as a function of (k, l) for

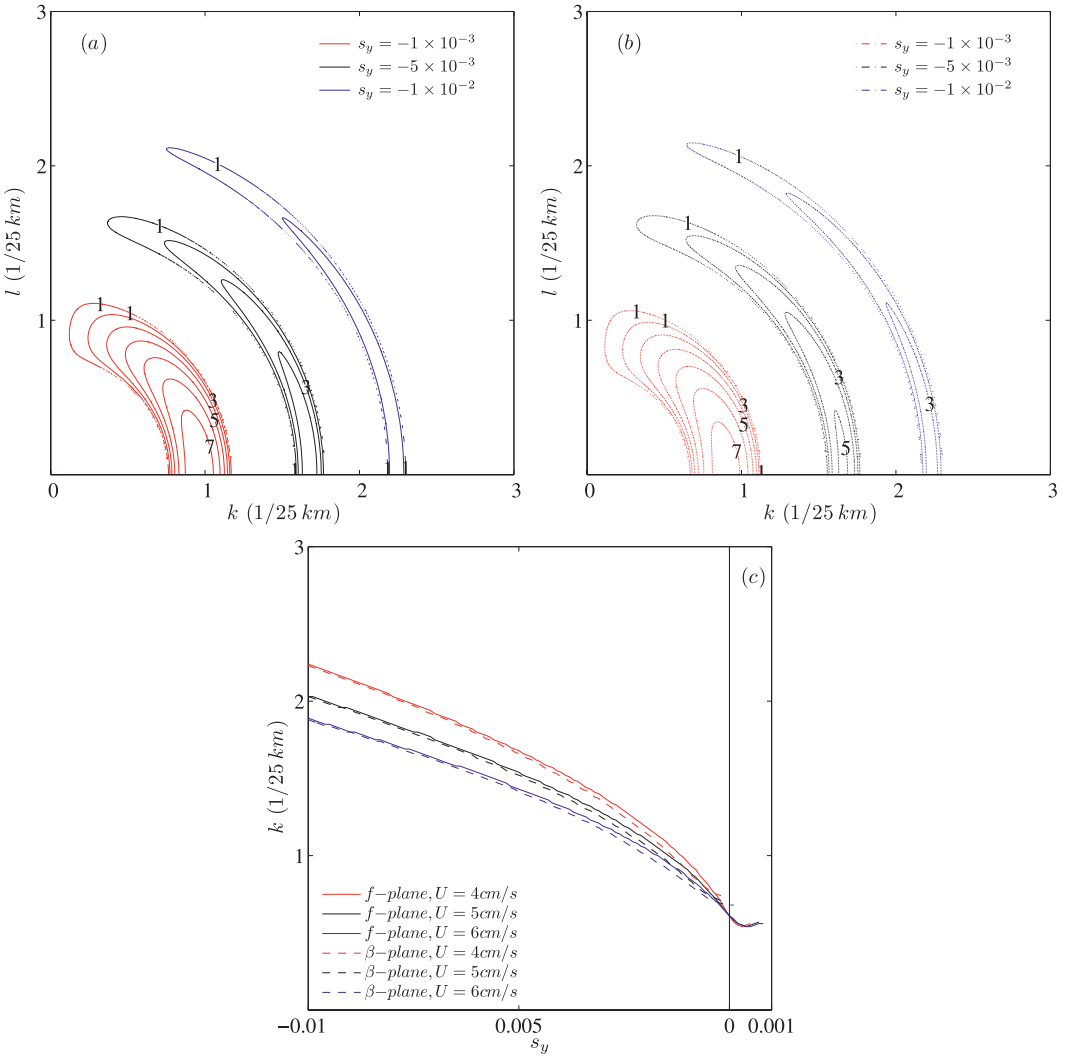

FIG. 1. Spatial structure of unstable modes in the presence of a meridional topographic slope. Greatest growth rates (yr^{-1}) of the unstable modes in the EB flow of 4 cm s^{-1} as a function of wavenumber for three different meridional slopes -10^{-3}, -5×10^{-3}, and -10^{-2} on the (a) f plane and (b) β plane. (c) Wavenumber of the most unstable mode as a function of the meridional slope for three different EB flows: 4, 5, and 6 cm s^{-1} on the f plane (solid lines) and β plane (dashed lines).

$U = 4$ cm s^{-1} over three negative (northward deepening) meridional slopes: weak -10^{-3}, intermediate -5×10^{-3}, and strong -10^{-2}. Note that the growth rate depends only on the magnitude of k and l, and the unstable waves are shown here within an incomplete annulus in the (k, l) plane. The greatest growth rate is found at $l = 0$; in other words, the most unstable mode is a meridional "noodle" mode. As the meridional slope gets steeper, the unstable wavenumber range moves away from the origin in the (k, l) plane, indicating shorter zonal and meridional wavelengths of the unstable modes, and becomes narrower. This inverse relationship between the steepness of the meridional slope and the zonal wavelength of the most unstable mode is further illustrated Fig. 1c. In contrast, the zonal wavelength of the most unstable mode increases with U.

Figure 2 shows the maximum growth rate and the corresponding phase speed as a function of the meridional slope for EB flows, $U = 4$, 5, and 6 cm s^{-1}. Interestingly, the maximum growth rate is found in the flat-bottom case ($S_y = 0$). Consistent with (14), a positive meridional slope (deepening southward) exerts a stabilizing effect on the EB flows, resulting in the decrease of the maximum growth rate and a complete elimination of the unstable modes as the slope becomes sufficiently steep. The corresponding "cutoff" value of the slope is

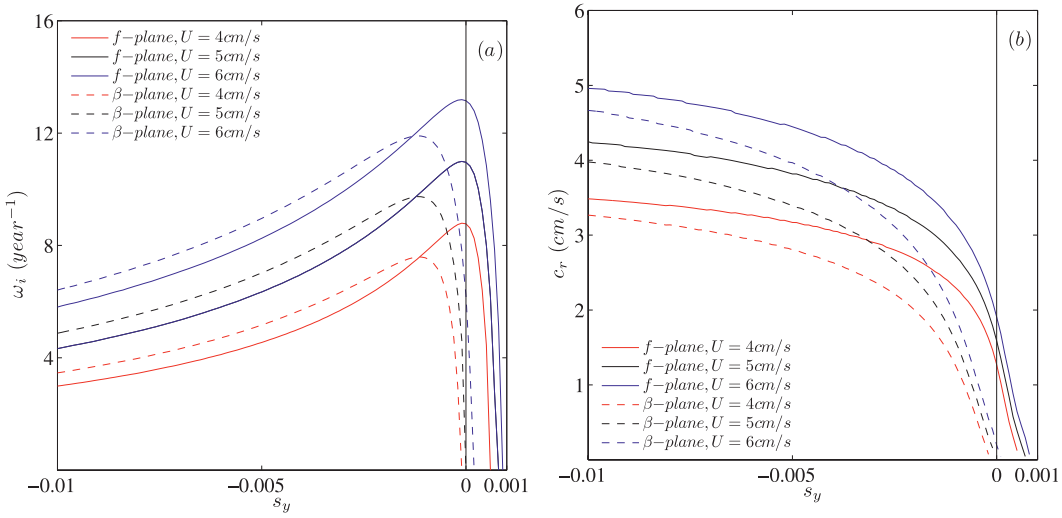

FIG. 2. Time dependence of the most unstable mode in the presence of a meridional topographic slope: (a) the greatest growth rate and (b) the corresponding phase speed for the EB flows with speeds of 4, 5, and 6 cm s^{-1} on the f plane (solid lines) and β plane (dashed lines).

determined by the necessary instability condition (13) and satisfies $S_y = UF_2$. As a negative (deepening northward) meridional slope becomes steeper, the maximum growth rate also decreases but remains positive (unstable). The corresponding phase speeds, as shown in Fig. 2b, increase in magnitude with the steepening of the negative meridional slope but remain smaller than U. The most unstable mode always propagates eastward, for both positive and negative zonal wavenumbers.

(ii) Zonal slope: $\beta_0 = 0$, $s_x \neq 0$ and $s_y = 0$

The effects of a zonal slope on the growth rates are similar to those of a meridional one (Fig. 3). In the flat-bottom case, unstable modes are found within a symmetric circle in the (k, l) plane, with the exception of $k = 0$. A zonal slope distorts the symmetry, and the unstable zonal wavelength becomes shorter. Additionally, slowly growing nearly zonally oriented modes with large meridional wavenumbers emerge at larger values of the slope. As in the case of a meridional slope, the unstable wavenumber interval (the shaded area in Fig. 3) shrinks as the slope becomes steeper, so in this sense the effects of the zonal slope can be interpreted as being stabilizing.

The zonal slope does not significantly influence the wavelengths, growth rate, and corresponding phase speed of the most unstable mode (figure not shown). The most unstable mode has a nearly meridional orientation with its zonal wavenumber exceeding its meridional one by an order of magnitude for several values of the main parameters ($U = 4, 5, 6$ cm s^{-1} and $H_2 = 3, 5$ km). The corresponding zonal wavelengths and phase speeds do not vary much, regardless of the magnitude of the zonal slope. This is consistent with the fact that the "noodle" mode is unaffected by the zonally sloping topography, as discussed earlier (see section 3a). The presence of both meridional and zonal slopes, as well as zonal slopes on the β plane (see the next section) can, however, significantly change the orientation of the most unstable mode.

In summary, as topographic slopes become stronger on the f plane, the unstable wavenumber interval shrinks and the unstable wavelengths tend to become shorter, especially for meridional slopes. The most unstable mode has a purely zonal wavevector for meridional slopes and a nearly zonal wavevector for purely zonal slopes. In the next section, we will see that the latter property will change on the β plane.

2) THE β PLANE

We next examine the effects of the interplay between the planetary vorticity gradient and topography on the linear baroclinic instability of a zonal flow. The β effect has a generally stabilizing influence on zonal currents. In particular, a flow over a flat bottom is no longer unstable for all values of U and can only support growing modes if its vertical shear exceeds a critical threshold. These critical shears, for our choice of parameters, are $-1.\dot{6}$ cm s^{-1} and 5.0 cm s^{-1}. In the following, "supercritical" refers to the shears with $U >$ 5.0 cm s^{-1} and $U < -1.\dot{6}$ cm s^{-1}, while "subcritical" refers to all other values of U. We will demonstrate that the subcritical values of the velocity shear can be destabilized by topography.

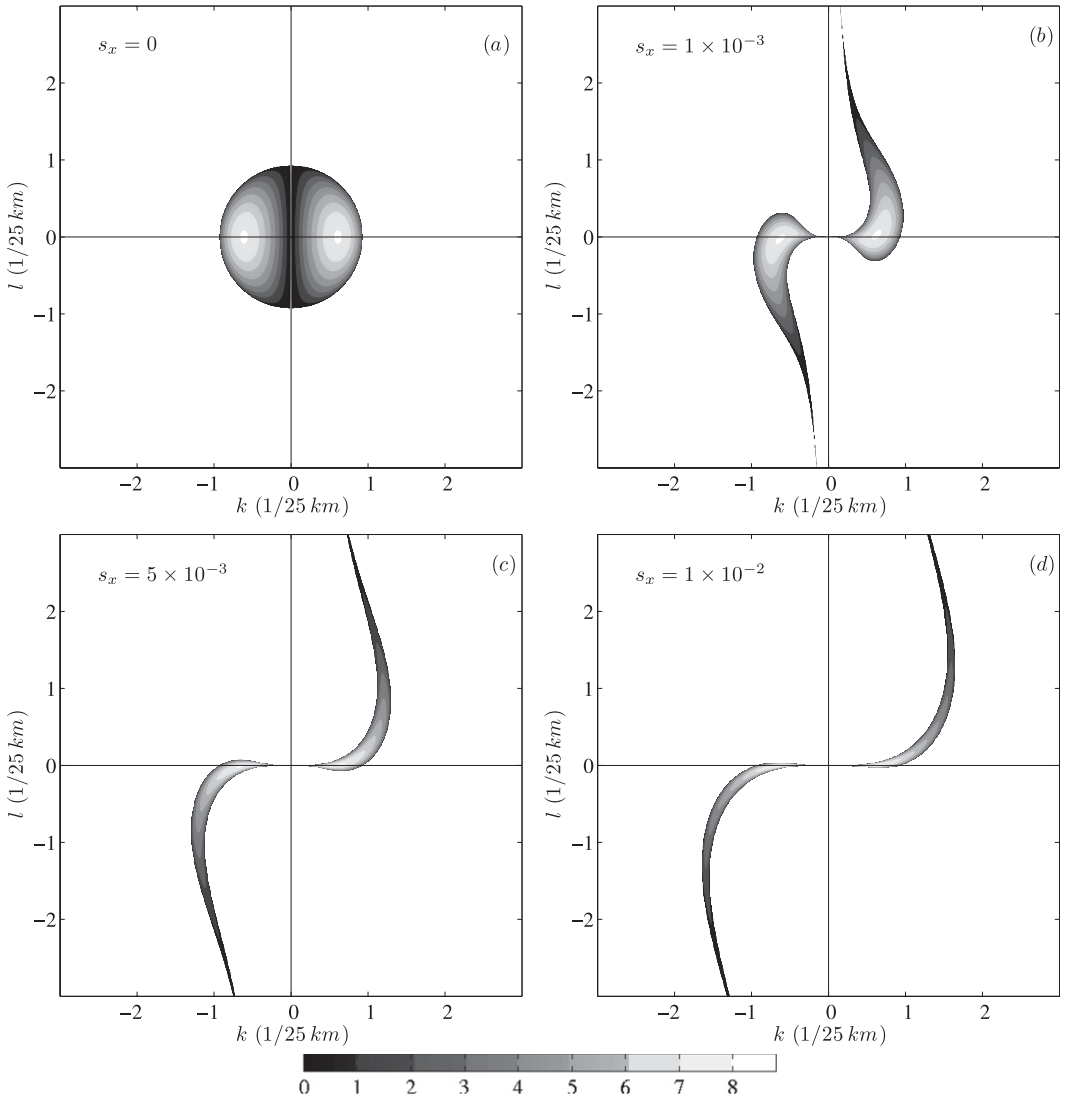

FIG. 3. Unstable modes in the presence of zonal slopes on the *f* plane: growth rates (yr^{-1}) as a function of the zonal and meridional wavenumber for zonal slopes (a) 0, (b) 1×10^{-3}, (c) 5×10^{-3}, and (d) 1×10^{-2} and the EB flow with a speed of 4 cm s^{-1}.

(i) Meridional slope: $\beta_0 \neq 0$, $s_x = 0$, and $s_y \neq 0$

As is discussed above, a meridional slope can stabilize a current by affecting the meridional PV gradient in the lower layer and preventing it from changing sign in the vertical. Alternatively, subcritical flows can become unstable because of the presence of a meridional slope. The analysis of an EB flow on the *f* plane is repeated here on the β plane and the results are plotted by the dashed lines in Figs. 1 and 2. Overall, the dependence of the wavelengths, growth rate, and phase speed of the most unstable mode on a meridional slope is very similar between the β and *f* planes. The results for westward background (WB) flows are also similar and not discussed here.

(ii) Zonal slope: $\beta_0 \neq 0$, $s_x \neq 0$, and $s_y = 0$

The effects of a zonal slope are considered next for three values of EB flows—subcritical (4 cm s^{-1}), critical (5 cm s^{-1}), and supercritical (6 cm s^{-1})—and WB flows for three supercritical values (−2, −3, and −4 cm s^{-1}). Positive (deepening westward) and negative (deepening eastward) zonal slopes with the same magnitude have the same effects on the greatest growth rate and the corresponding phase speed; this is because two pairs of oppositely signed l/k and s_x correspond to the same κ and, consequently, the same solution to the dispersion relation. Thus, we only consider positive zonal slopes in the following analysis.

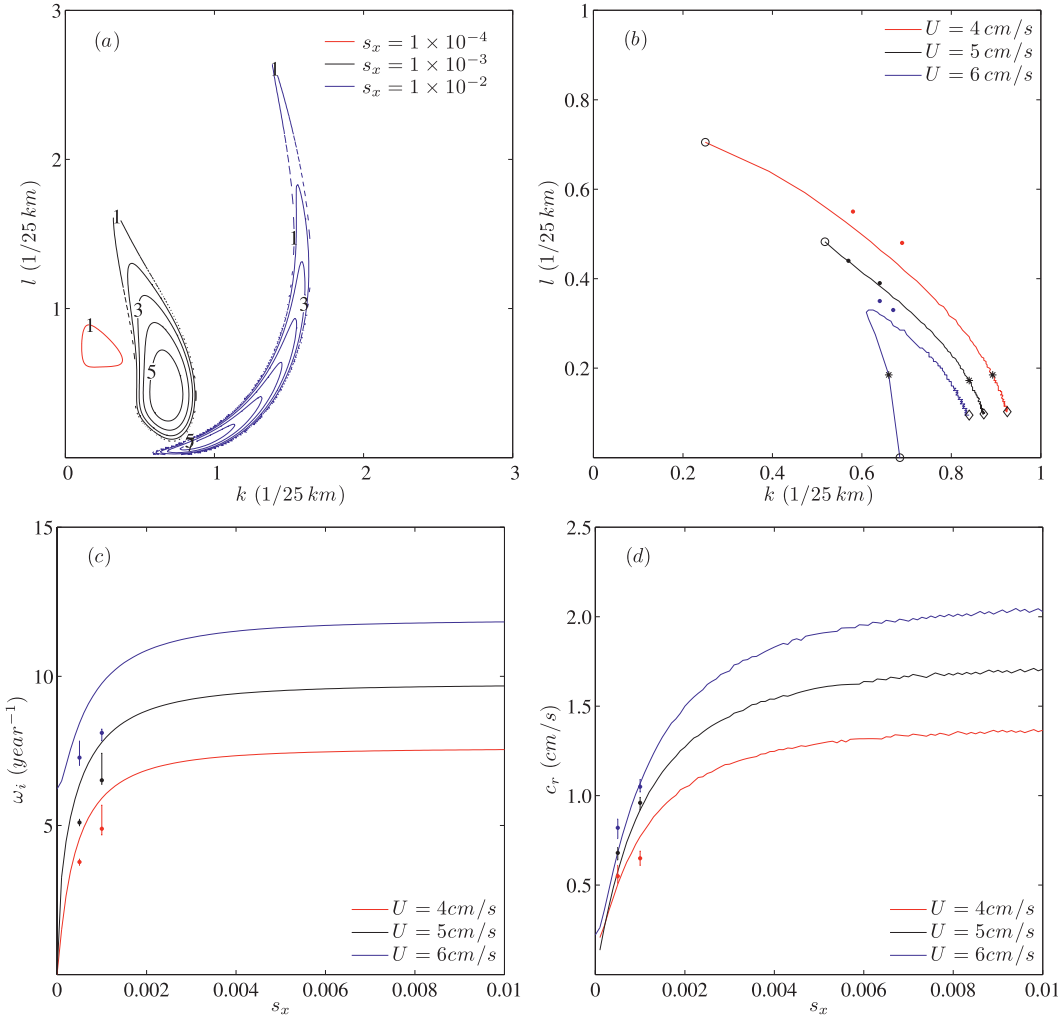

FIG. 4. Unstable modes in the presence of a zonal topographic slope and EB flows on the β plane. (a) The greatest growth rates (yr^{-1}) for the EB flow with a speed of 4 cm s^{-1} as a function of the zonal and meridional wavenumber for the three zonal slopes 10^{-4}, 10^{-3}, and 10^{-2}. (b) The wavenumber of the most unstable mode for $U = 4$, 5, and 6 cm s^{-1} as a function of the zonal slope, which increases along the curves and three values are shown: 10^{-4} (open circles), 10^{-3} (asterisks), and 10^{-2} (diamonds); the dots being the results from numerical simulations for $s_x = 5 \times 10^{-4}$ and 10^{-3} and the three different EB flows. (c) The greatest growth rate in curves and the numerical results (dots with error bars) for $s_x = 5 \times 10^{-4}$ and 10^{-3} and the three different EB flows and (d) the corresponding phase speed and the numerical results (dots with error bars) for $s_x = 5 \times 10^{-4}$ and 10^{-3} and for the same values of U.

Even a small zonal slope can destabilize a subcritical zonal background flow. For example, a small zonal slope of 10^{-4} makes a current with $U = 4$ cm s^{-1} unstable in a limited range of wavenumbers (red contours in Fig. 4a). The unstable wavenumber range increases substantially when the zonal slope is as large as 10^{-3} (black contours). As the zonal slope gets even larger, unstable wavenumbers are squeezed into a narrow wavenumber interval similar to that observed on the f plane. The unstable wavenumber range changes in a similar manner for the supercritical flow of $U = 6$ cm s^{-1} and large slopes. In contrast, smaller values of U correspond to very narrow unstable wavenumber ranges (figure not shown).

Unlike a zonal/meridional topographic slope on the f plane or a meridional topographic slope on the β plane, a zonal slope on the β plane modifies the shape of the most unstable mode, which is no longer the meridionally oriented "noodle" mode. Figure 4b shows the zonal and meridional wavenumbers of the most unstable mode as the zonal slope increases from 0 to 10^{-2} and for $U = 4$, 5, and 6 cm s^{-1}. As expected, only the supercritical flow $U = 6$ cm s^{-1} is unstable at a zonal slope of 0, where the most unstable mode has the shape of a meridional

"noodle" mode ($l = 0$). The wavevector of the most unstable mode for $U = 6$ cm s^{-1} (blue curve) rotates first counterclockwise in the (k, l) plane as the zonal slope increases, changing from a meridional "noodle" mode ($l = 0$) to a slanted mode ($l \approx k$), and then clockwise for very large slopes. For the subcritical/critical shears $U = 4$ and 5 cm s^{-1}, unstable modes start emerging for a zonal slope as small as 10^{-4} and the most unstable wavevector rotates clockwise in the (k, l) plane, changing its orientation from nearly meridional to nearly zonal.

In contrast to the f plane, as shown in Figs. 4c and 4d, the growth rate of the most unstable mode increases sharply with the zonal slope, before approaching a nearly constant value at the slope of $\sim 5 \times 10^{-3}$. The phase speed exhibits similar behavior and remains eastward for both negative and positive values of k.

Several effects of a zonal slope on WB flows on β plane are qualitatively similar to those of supercritical EB flows (Fig. 5). In particular, the range of unstable wavenumbers shrinks as the slope magnitude increases (Fig. 5). The growth rate increases, and the wavevector of the most unstable mode rotates counterclockwise as the slope gets larger (Fig. 5d). The most unstable mode of a WB flow also propagates downstream (westward), but its phase speed magnitude decreases with the zonal slope (figure not shown).

(iii) Vertical structure

The vertical structure of the most unstable mode shows a strong dependence on meridional and zonal slopes. The most unstable mode becomes more surface intensified as a negative meridional slope becomes steeper. As shown in Fig. 6a the ratios between the amplitudes of the most unstable mode in the top (A_1) and bottom (A_2) layers for $U = 4$ and 6 cm s^{-1} increase sharply with the slope magnitude. These changes are explained by the increase in the relative importance of the baroclinic component of the mode. The corresponding ratio between the barotropic mode $A_b = (A_1H_1 + A_2H_2)/(H_1 + H_2)$ and the residual baroclinic one in the upper layer $A_z = A_1 - A_b$ is shown in Fig. 6b. Although this ratio is about 1 when the meridional slope is very small, it decreases to less than 0.5 as the slope becomes steeper.

A zonal slope exerts distinct effects on subcritical and supercritical background flows. For the subcritical EB flow of 4 cm s^{-1} A_1 and A_2 are nearly the same when the zonal slope is very small (Fig. 7a). As in the case of a meridional slope, the most unstable mode becomes more surface intensified as the zonal slope gets larger, but this effect is weaker than in the case of a meridional slope, and A_1/A_2 reaches a nearly constant value of about 4.5. These changes are attributed to the increase in the relative importance of the baroclinic component of the mode; although the barotropic component tends to dominate over the baroclinic one for all slopes, A_b/A_z decreases sharply from more than 5 to almost 1, as the zonal slope increases (Fig. 7b). For the supercritical EB flow of 6 cm s^{-1}, as in the subcritical case, the most unstable mode is surface intensified for all zonal slopes. The ratio A_1/A_2 decreases slightly in the beginning, but increases afterward as the zonal slope increases. In contrast to the subcritical case, however, A_b/A_z for $U = 6$ cm s^{-1} is around 1 for all zonal slopes, indicating a mix of barotropic and baroclinic components of the most unstable mode. Changes in a negative zonal slope lead to a similar dependence.

c. Effects of the orientation of the background PV gradients

The largest dynamical effect of the introduction of a zonal topographic slope is to make the background PV gradient in the lower layer nonmeridional. The effects of this rotation on the most unstable mode are explicitly explored in this section, by keeping the magnitude of the PV gradient fixed, but changing its orientation. This is readily achieved by changing S_x and S_y simultaneously. The spatial structure of the most unstable mode is characterized by the orientation of the wavevector (k, l) with respect to the y axis and denoted as angle θ_{kl}. For example, $\theta_{kl} = 90°$ corresponds to a meridional "noodle" mode.

We follow Flierl (1978) and define barotropic and baroclinic potential vorticity, q_{BT} and q_{BC} in the following way:

$$q_{\mathrm{BT}} = \alpha_2 q_1 + \alpha_1 q_2, \tag{18}$$

$$q_{\mathrm{BC}} = \sqrt{\alpha_1\alpha_2}(q_1 - q_2). \tag{19}$$

The barotropic and baroclinic PV gradients, ∇q_{BT} and ∇q_{BC} are

$$\nabla q_{\mathrm{BT}} = \alpha_1 S_x \mathbf{i} + (\beta_0 + \alpha_1 S_y)\mathbf{j}, \tag{20}$$

$$\nabla q_{\mathrm{BC}} = -\sqrt{\alpha_1\alpha_2} S_x \mathbf{i} + \sqrt{\alpha_1\alpha_2}(FU - S_y)\mathbf{j}. \tag{21}$$

We begin by examining the relationship between θ_{kl} and the orientation of the barotropic PV gradient, quantified by $\theta_{\nabla q_{\mathrm{BT}}}$, the angle between this gradient and the x axis ($\theta_{\nabla q_{\mathrm{BT}}} = 90°$ in the absence of topography). Note that $\theta_{\nabla q_{\mathrm{BT}}} = \theta_{kl}$ means that the wavevector is perpendicular and the velocity vector is parallel to the direction of the barotropic PV gradient. We are also interested in how the relationship between θ_{kl} and $\theta_{\nabla q_{\mathrm{BT}}}$

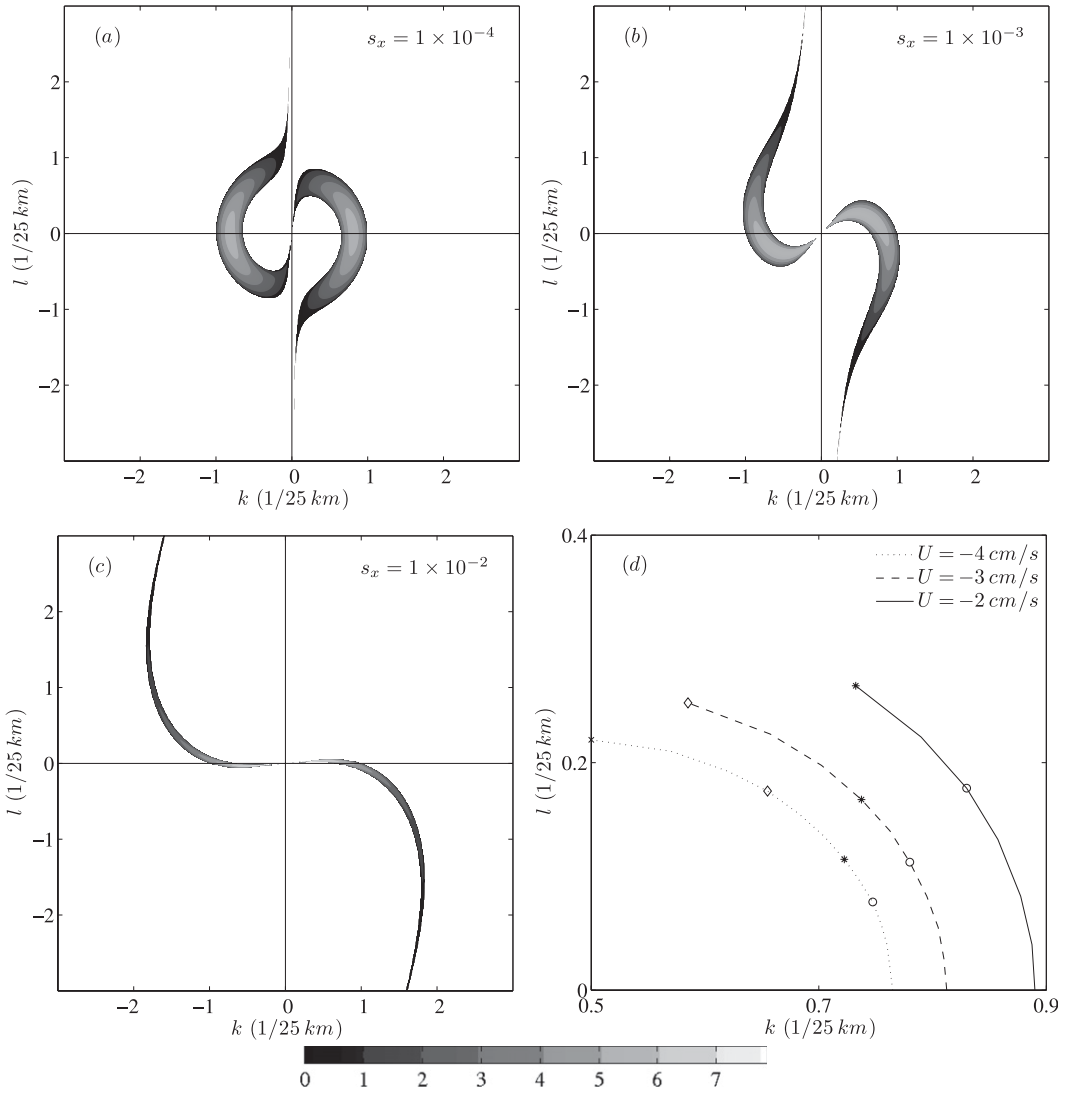

FIG. 5. Unstable modes in the presence of a zonal topographic slope and WB flows on the β plane. Growth rate (yr^{-1}) as a function of the zonal and meridional wavenumber is shown for different zonal slopes: (a) 1×10^{-4}, (b) 1×10^{-3}, and (c) 1×10^{-2} for the WB flow with a speed of -3 cm s^{-1}. (d) Wavenumber of the most unstable mode for $U = -4$, -3, and -2 cm s^{-1}—the zonal slope increases along the curves and four values are shown: 5×10^{-4} (circles), 7×10^{-4} (asterisks), 1.1×10^{-3} (diamonds), and 1.3×10^{-3} (cross); beyond the slope value of $\sim 10^{-3}$, it becomes very difficult to accurately calculate the wavelength of the most unstable mode, because unstable modes are found in an increasingly narrow interval near the origin in the (k, l) plane and the corresponding growth rates are too close to be distinguished within the computation accuracy.

is affected by the vertical shear and stratification. For this purpose, we will also vary U and H_2.

First, we consider three EB flows: weak (1 cm s^{-1}), intermediate (6 cm s^{-1}), and strong (12 cm s^{-1}), while keeping the depths of the two isopycnal layers $H_1 = 1$ km and $H_2 = 3$ km. We maintain the same magnitude of ∇q_{BT} as $2\beta_0$ and rotate it from northward (90°) to eastward (0°) directions by changing the bottom slopes from $(S_x, S_y) = (0, \beta_0, \alpha_1)$ to $(S_x, S_y) = (2\beta_0/\alpha_1, -\beta_0/\alpha_1)$.

Both EB flows of 1 and 6 cm s^{-1} are stable when ∇q_{BT} points to the north with a purely meridional slope. A very small zonal component of the PV gradient ($\theta_{\nabla q_{\mathrm{BT}}}$ is slightly less than 90°), however, destabilizes these flows, and the most unstable mode is nearly zonally oriented and has an almost meridional wavevector (θ_{kl} is close to 0°). For the EB flow of 1 cm s^{-1}, as ∇q_{BT} becomes more zonal, θ_{kl} is always shifted by 90° with respect to $\theta_{\nabla q_{\mathrm{BT}}}$ (red line in Fig. 8a). This indicates that the most unstable wavevector is parallel to the barotropic PV gradient for

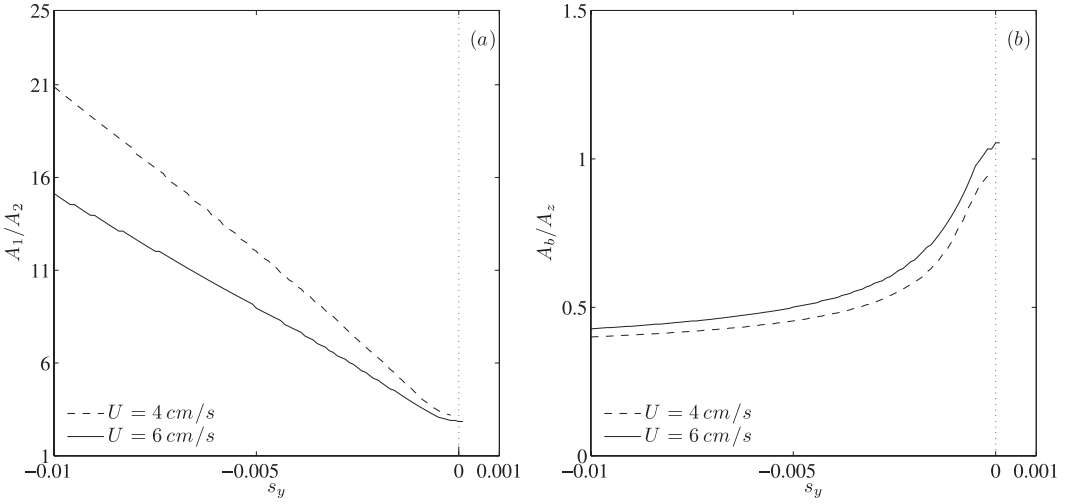

FIG. 6. Vertical structure of the most unstable modes in the case of EB flows over meridional topographic slopes: (a) ratio between the magnitude of the upper and lower layer streamfunctions for $U = 4$ and 6 cm s^{-1} as a function of the meridional slope and (b) the corresponding ratio between the barotropic and the baroclinic modes in the upper layer.

a background flow as weak as 1 cm s^{-1}. A similar situation is observed for $U = 4$ cm s^{-1} and small zonal slopes in the previous section. For a stronger background velocity shear of 6 cm s^{-1}, this parallel orientation of the most unstable wavevector and the barotropic PV gradient is less obvious.

The EB flow of 12 cm s^{-1} is, in contrast, baroclinically unstable when the barotropic PV gradient is purely meridional ($\theta_{\nabla q_{\rm BT}} = 90°$) and θ_{kl} is also 90° (the meridional ''noodle'' mode); the velocity vector is parallel to $\nabla q_{\rm BT}$. This is a typical situation for the modes growing in the baroclinic shear, as this orientation enables these modes to most efficiently extract energy from the background state (Pedlosky 1987). For nonzero zonal slopes, the difference between θ_{kl} and $\theta_{\nabla q_{\rm BT}}$ increases. When the PV gradient is zonal ($\theta_{\nabla q_{\rm BT}} = 0$), this difference is 90° and the wavevector is parallel to the PV gradient.

The relationship between the barotropic PV gradient and the most unstable wavevector is sensitive to the mean stratification. We consider here the EB flow of 6 cm s^{-1} and three different values of H_2: 1, 3, and 5 km. The upper layer is 1 km for all the three cases. These values can be interpreted as the cases with thermoclines that are deep, intermediate, and shallow in comparison to the total depth of the ocean. Note that, when the

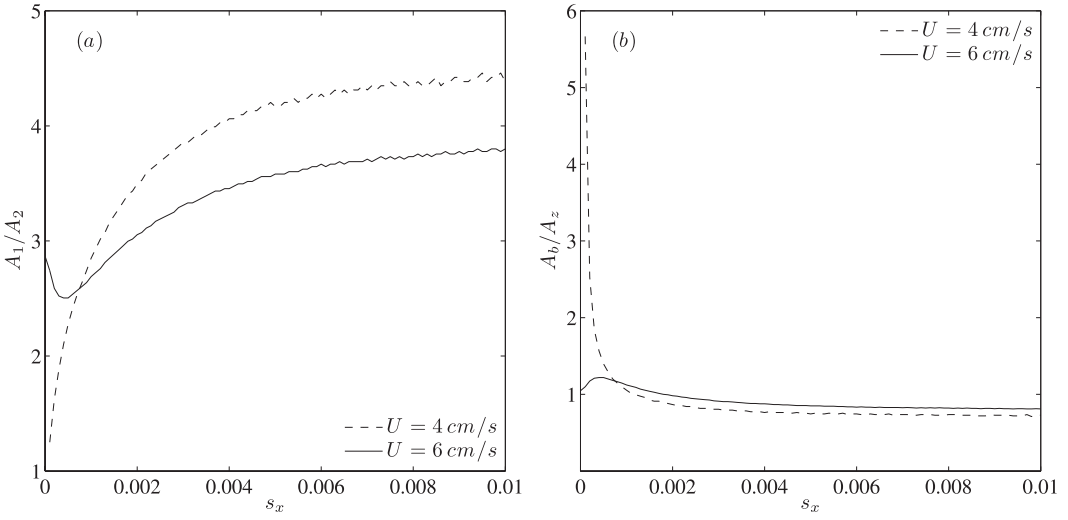

FIG. 7. As in Fig. 6, but over zonal topographic slopes and the ratio as a function of the zonal slope.

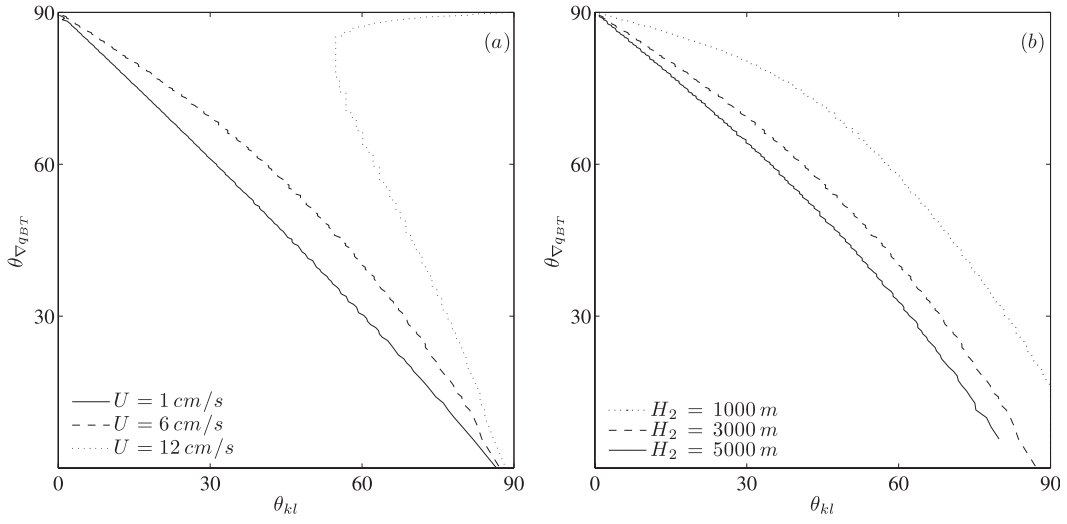

FIG. 8. Orientation of the wavevectors and the barotropic PV gradient for (a) three EB flows, $H_2 = 3$ km, and (b) the EB flow with a speed of 6 cm s^{-1} and three different values of H_2.

bottom is flat, a larger H_2 (and smaller α_2) implies an increased stability of the background flows. For a deep lower layer of 5 km, θ_{kl} is always nearly parallel to $\nabla q_{\rm BT}$ (Fig. 8b). The difference between $\theta_{\nabla q_{\rm BT}}$ and θ_{kl} shifts away from 90° as the lower layer becomes thinner (black and red curves).

The relationship between θ_{kl} and $\theta_{\nabla q_{\rm BC}}$ has also been examined, but the former angle does not appear to be sensitive to the orientation of the baroclinic PV gradient and is not discussed here.

4. Meridional ridge: Numerical results

The linear baroclinic instability properties of zonal flows over topography are studied next in a linearized numerical QG model. The model is exactly the one described in section 2, except it is confined in a zonally reentrant channel centered at 45°N. Its meridional width is $L_y = 3600$ km; its zonal length is $L_x = 4L_y$. Grid resolution is 7 km. This numerical code is adapted from Berloff et al. (2009a) with nonlinear advection terms turned off. All parameters are the same as those used in section 3. The model is initialized with random perturbations, among which some wavenumbers become unstable and grow exponentially.

By assuming that the most unstable mode tends to dominate the flow evolution in the model at long times, we can estimate the growth rate, phase speed, and spatial structure of the most unstable mode. Specifically, we calculate the growth rate from the last 100 days of each simulation (before the model becomes numerically unstable) by fitting an exponent into the energy time evolution. The phase speed is estimated from the slope of Hovmöller diagrams during the same time period. Errors in both the growth rate and phase speed are estimated by bootstrapping. The zonal and meridional wavelengths of the most unstable mode are determined by eye, by counting the number of maxima (as in Fig. 9b). Note that the model domain allows only a discrete set of wavenumbers: consequently, the model may not permit the analytically most unstable mode. This bias is, however, found to be not significant in the cases considered below. The ability of these methods to capture the main properties of the most unstable modes is first verified in the case of a constant topographic slope. The corresponding linear numerical

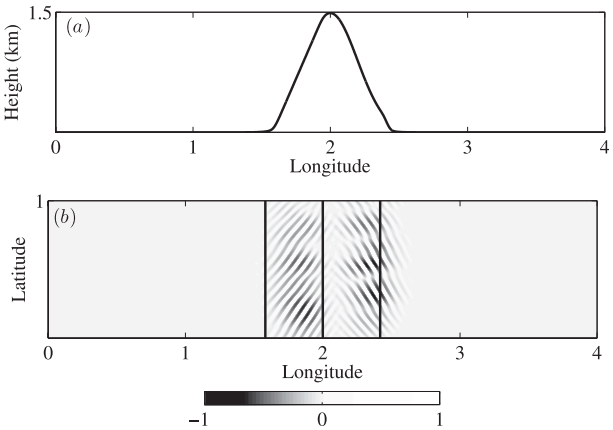

FIG. 9. Linear numerical results: (a) schematic of the meridional ridge and (b) the disturbance streamfunction for the EB flow with a speed of 4 cm s^{-1}, scaled to the streamfunction magnitude; vertical black lines denote positions of the edges and center of the ridge. These most unstable mode are patchy instead of being uniform due to boundary effects of the channel walls.

solutions are very close to those from the analytical dispersion relation of Eq. (15). Specifically, the growth rate from the model is only 4% smaller than the analytical one; the wavelength and phase speed of the most unstable mode are also nearly the same as the analytical values.

We next proceed with a numerical analysis of the linear solutions over a topographic ridge and examine the extent to which the unstable modes, developing in the presence of the ridge, can be described using our analytical results with a constant zonal slope. We need to point out that the numerical results, even in the vicinity of the ridge itself can, in general, be very different from the analytical ones due to the more complicated topography and boundary conditions in the former case. We, however, find that the numerical solutions are generally consistent with the local stability properties from theory. The numerical results for several parameters are shown in Figs. 4b–d by solid dots with error bars.

We begin with the EB flow of 4 cm s^{-1} over a ridge with the slopes of $\pm 10^{-3}$, which is subcritical over a flat bottom. The meridional ridge is shown in Fig. 9a; it has a height of 1500 m and a width of 3000 km. The numerical results exhibit slanted orientations on both sides of this symmetric ridge and very small amplitudes over the flat bottom section of the channel (Fig. 9b). The spatial structure of this numerical solution closely matches that of the most unstable mode from the analytical model with a constant zonal slope of 10^{-3}. Specifically, the wavevector (scaled by the internal Rossby deformation radius) of the most unstable mode from the numerical simulation is $(k, l) = (0.69, 0.48)$, which is very close to the analytical result $(k, l) = (0.68, 0.43)$ for the positive (eastward deepening) slope of 10^{-3} (Fig. 4b). The negative slope corresponds to the oppositely signed l. The calculated growth rate is 4.89 yr^{-1}, which is somewhat lower than the analytical one, 5.91 yr^{-1} (Fig. 4c). This can also be partly due to the fact that several unstable modes grow in this simulation together with the most unstable mode, but at lower rates. Nearly negligible motions away from the ridge are also consistent with *local* stability properties of this subcritical current, which is stable over the flat bottom. The propagating speed of the most unstable mode is 0.0065 m s^{-1} and eastward, which is slightly lower than the analytical result of 0.0076 m s^{-1}. We remind the reader that the most unstable wave modes over the negative and positive zonal slopes of the ridge propagate eastward with the same phase speed.

The results for the meridional ridges with slopes of $\pm 5 \times 10^{-4}$ and $\pm 10^{-3}$ and the EB flows $U = 4$, 5, and 6 cm s^{-1} are also generally consistent with local stability properties. In particular, unstable modes exhibit slanted structures over the ridges; away from the ridges, the amplitudes are very small, and the meridional ''noodle'' mode in the flat-bottom case is not visible. In other words, the disturbances are strongly trapped to the ridges. This is generally consistent with the growth rates over a flat bottom being significantly smaller than those over a zonal slope (Fig. 4). The growth rates of the numerical solutions are 13%–19% lower than the analytical ones, and the phase speeds are within 20% of the analytical ones. Other experiments configured with different topographic features, such as a double ridge and a trough, exhibit a similar agreement with the local analytical results (figures not shown).

5. Summary and conclusions

This study demonstrates the importance of bottom topography in the linear baroclinic instability of oceanic currents. Constant topographic slopes are shown to significantly modify stability properties of zonal flows, through the changes in the background PV gradient. A zonal slope introduces a zonal component in the PV gradient, which has a strong destabilizing effect on the flow: this is also consistent with the enhanced eddy kinetic energy over zonal slopes found by Boland et al. (2012). In particular, even a small zonal slope can destabilize a flow that is otherwise stable in the absence of topography, and the growth rates of the most unstable modes increase with the magnitude of the slope. In contrast, a meridional slope can stabilize/destabilize a zonal flow only through changing the background PV gradient in the lower layer beyond a known threshold.

The spatial structure of the fastest-growing modes is also sensitive to the orientation of topographic slopes. The importance of the baroclinic component of the most unstable mode increases with the increase of zonal slope magnitude, and the mode becomes surface intensified. Surface-intensified modes are also found in a linear two-layer QG model in Samelson (1992), in which the horizontal scales of the topography are comparable to that of the waves, and in Hallberg (1997), where they become coupled with bottom-intensified flows when the topographic gradient is meridional. Northward- or zonally sloping topography in our study also leads to the shortening of the most unstable wavelength, in comparison with the flat bottom.

When the slope is purely meridional or zero, the most unstable mode has the shape of a meridional ''noodle'' mode and the wavevector has a purely zonal orientation. This orientation allows the most efficient extraction of energy from the background stratification (Pedlosky 1987). The introduction of the zonal slope causes the most unstable modes to become slanted horizontally. The relationship between the PV gradient and the

orientation of the most unstable wavenumber depends on how stable (subcritical) the zonal flow is. For a weak zonal flow or a thick lower layer, the orientation of the wavevector is parallel (and the velocity vector is perpendicular) to the barotropic PV gradient, which indicates a strong topographic control on the mode orientation. A similar and strong relationship between eddy-driven jets and the barotropic PV gradient is reported by Boland et al. (2012). This is consistent with the mechanism of jet formation proposed by Berloff et al. (2009a), in which jets form as a result of the secondary instability of the primary unstable modes; in their model with a flat bottom the jets are perpendicular to the most unstable ''noodle'' modes of the linear problem. Most unstable modes in strong (supercritical) currents, in contrast, exhibit a weak relation between the orientations of their wavevector and the barotropic PV gradient. These wavevectors, instead, appear to be primarily controlled by the direction of the velocity shear.

The results of the linearized numerical simulations with meridional ridges/troughs are generally consistent with the local stability properties. In particular, the dominant growing solution is localized to the ridge and has the spatial structure and growth rate consistent with those predicted by the linear theory over a constant zonal slope. This ''trapping'' of the modes to the ridge can be explained by the enhanced instability due to the zonal slopes on the sides of the ridge. The entire growing anomaly propagates to the east in the eastward background current and to the west in the westward one. During the nonlinear evolution stage, one can therefore expect coherent structures to form downstream of the ridge. This result may help explain the highly energetic eddy activity downstream of topography observed in Thompson and Sallée (2012) and our nonlinear simulation. This property can also have important implications for the formation of the eddy-driven jets next to the meridional ridges, which is observed in our nonlinear study (in progress).

The results of this idealized study can help to interpret eddy generation over more complex topographic features in the real ocean and more sophisticated numerical models. The demonstrated importance of topography strongly suggests that the traditional stability analysis based entirely on the vertical shear in zonal ocean currents is insufficient for predicting the basic properties of growing disturbances. Topography, as well as such features of the mean current as its nonzonal orientation and spatial variability, can be expected to be critical factors in oceanic eddy generation.

Acknowledgments. The authors are thankful to Pavel Berloff for his help with the numerical simulations and to Romain Pennel and an anonymous reviewer for their input on the text. This study was supported by the National Science Foundation, Grant OCE-0842834.

REFERENCES

Benilov, E. S., 2001: Baroclinic instability of two-layer flows over one-dimensional bottom topography. *J. Phys. Oceanogr.,* **31,** 2019–2025.

Berloff, P., I. Kamenkovich, and J. Pedlosky, 2009a: A mechanism of formation of multiple zonal jets in the oceans. *J. Fluid Mech.,* **628,** 395–425.

——, ——, and ——, 2009b: A model of multiple zonal jets in the oceans: Dynamical and kinematical analysis. *J. Phys. Oceanogr.,* **39,** 2711–2734.

Blumsack, S. L., and P. J. Gierasch, 1972: Mars—The effects of topography on baroclinic instability. *J. Atmos. Sci.,* **29,** 1081–1089.

Boland, E. J. D., A. F. Thompson, E. Shuckburgh, and P. H. Haynes, 2012: The formation of nonzonal jets over sloped topography. *J. Phys. Oceanogr.,* **42,** 1635–1651.

Flierl, G. R., 1978: Models of vertical structure and the calibration of two-layer models. *Dyn. Atmos. Oceans,* **2,** 341–381.

Hallberg, R., 1997: Localized coupling between surface and bottom-intensified flow over topography. *J. Phys. Oceanogr.,* **27,** 977–998.

Hart, J. E., 1975a: Baroclinic instability over a slope. Part I: Linear theory. *J. Phys. Oceanogr.,* **5,** 625–633.

——, 1975b: Baroclinic instability over a slope. Part II: Finite-amplitude theory. *J. Phys. Oceanogr.,* **5,** 634–641.

Isachsen, P. E., 2011: Baroclinic instability and eddy tracer transport across sloping bottom topography: How well does a modified Eady model do in primitive equation simulations? *Ocean Modell.,* **39,** 183–199.

Kamenkovich, I., and J. Pedlosky, 1996: Radiating instability of nonzonal ocean currents. *J. Phys. Oceanogr.,* **26,** 622–643.

——, P. Berloff, and J. Pedlosky, 2009: Role of eddy forcing in the dynamics of multiple zonal jets in a model of the North Atlantic. *J. Phys. Oceanogr.,* **39,** 1361–1379.

Kondratyev, K., and G. Hunt, 1982: *Weather and Climate on Planets.* Elsevier, 768 pp.

Maximenko, N. A., B. Bang, and H. Sasaki, 2005: Observational evidence of alternating zonal jets in the world ocean. *Geophys. Res. Lett.,* **32,** L12607, doi:10.1029/2005GL022728.

Mechoso, C. R., 1980: Baroclinic instability of flows along sloping boundaries. *J. Atmos. Sci.,* **37,** 1393–1399.

Melnichenko, O. V., N. A. Maximenko, N. Schneider, and H. Sasaki, 2010: Quasi-stationary striations in basin-scale oceanic circulation: Vorticity balance from observations and eddy-resolving model. *Ocean Dyn.,* **60,** 653–666.

Nakano, H., and H. Hasumi, 2005: A series of zonal jets embedded in the broad zonal flows in the Pacific obtained in eddy-permitting ocean general circulation models. *J. Phys. Oceanogr.,* **35,** 474–488.

Nowlin, W. D., and J. M. Klinck, 1986: The physics of the Antarctic Circumpolar Current. *Rev. Geophys.,* **24,** 469–491.

Orsi, A. H., T. Whitworth, III, and W. D. Nowlin Jr., 1995: On the meridional extent and fronts of the Antarctic Circumpolar Current. *Deep-Sea Res.,* **42,** 641–673.

Panetta, R. L., 1993: Zonal jets in wide baroclinically unstable regions: Persistence and scale selection. *J. Atmos. Sci.,* **50,** 2073–2106.

Pedlosky, J., 1987: *Geophysical Fluid Dynamics.* 2nd ed. Springer, 710 pp.

Pennel, R., A. Stegner, and K. Béranger, 2012: Shelf impact on buoyant coastal current instabilities. *J. Phys. Oceanogr.,* **42,** 39–61.

Reznik, G. M., and T. B. Tsybaneva, 1999: Planetary waves in a stratified ocean of variable depth. Part 1. Two-layer model. *J. Fluid Mech.,* **388,** 115–145.

Rhines, P. B., 1994: Jets. *Chaos,* **4,** 313–339.

Richards, K. J., N. A. Maximenko, F. O. Bryan, and H. Sasaki, 2006: Zonal jets in the Pacific Ocean. *Geophys. Res. Lett.,* **33,** 4–7.

Samelson, R. M., 1992: Surface-intensified Rossby waves over rough topography. *J. Mar. Res.,* **50,** 367–384.

——, and J. Pedlosky, 1990: Local baroclinic instability of flow over variable topography. *J. Fluid Mech.,* **221,** 411–436.

Sokolov, S., and S. R. Rintoul, 2007: Multiple jets of the Antarctic Circumpolar Current south of Australia. *J. Phys. Oceanogr.,* **37,** 1394–1412.

Steinsaltz, D., 1987: Instability of baroclinic waves with bottom slope. *J. Phys. Oceanogr.,* **17,** 2343–2350.

Thompson, A. F., 2010: Jet formation and evolution in baroclinic turbulence with simple topography. *J. Phys. Oceanogr.,* **40,** 257–278.

——, and J.-B. Sallée, 2012: Jets and topography: Jet transitions and the impact on transport in the Antarctic Circumpolar Current. *J. Phys. Oceanogr.,* **42,** 956–972.

Vallis, G. K., and M. E. Maltrud, 1993: Generation of mean flow and jets on a beta-plane and over topography. *J. Phys. Oceanogr.,* **23,** 1346–1362.

van Sebille, E., I. Kamenkovich, and J. K. Willis, 2011: Quasi-zonal jets in 3-D Argo data of the northeast Atlantic. *Geophys. Res. Lett.,* **38,** L02606, doi:10.1029/2010GL046267.